Bulgarian Journal of Physics vol. **49** (2022) 362–374

Structural, Electrical and Magnetic Properties of Zn Doped $NiFe_2O_4$ Added with 0.8wt%V_2O_5 Synthesized via Ceramic Method

Madhukar S. Patil*

Department of Physics, Yashwantrao Chavan College, Sillod, Aurangabad, India
*Corresponding author E-mail: mspatil9827@gmail.com

Received *23 December 2021*, Revised *27 June 2022*

doi: https://doi.org/10.55318/bgjp.2022.49.4.362

Abstract. Using the traditional ceramic process, zinc doped 'Nickel ferrite' with V_2O_5 was produced, yielding $Ni_{0.7}Zn_{0.3}Fe_2O_4 + 0.8wt\%V_2O_5$. Various technical methodologies were used to characterize structural, electrical, magnetic, and dielectric properties. X-ray diffraction was used to identify the crystalline phases after the addition of V_2O_5 as an impurity. Major reflections obtained in XRD were indexed as (220), (310), (311), (222), (400), (422), (511), and (440) planes that confirmed the formation of ferrite crystalline phases in particular with single-phase, cubic shape, spinel structure. The avg. lattice parameter (a) of the prepared sample was found to be 8.380±0.005 Å. The X-ray density was recorded to be 5.303 g/cm^3. The crystallite size (t) was calculated by using the Debye-Scherrer method taking the (311) plane of maximum intensity; it was reported to be 2.684 μm. The development of the ferrite phase was supported by different absorption bands v_1 (542 cm^{-1}) and v_2 (410.84 cm^{-1}) corresponding to the tetrahedral and octahedral group complexes Fe^{3+}–O^{2-} respectively. The logarithmic plot of DC resistivity has shown the semiconducting behaviour of the prepared samples. The magnetic parameters have shown some changes at higher levels after the addition of V_2O_5 in $Ni_{0.7}Zn_{0.3}Fe_2O_4$.

KEY WORDS: Nickel ferrite, ceramic method, V_2O_5, X-diffraction, magnetic property.

1 Introduction

Magnetic materials are currently popular due to their uncompensated physico-chemical properties, which make them stand out in a variety of applications. Following the challenges in the scientific and technological domains, the global demand for novel materials and spinel ferrites is expanding linearly. Due to their possessive semiconducting activity, electro-magnetic nature, electrochemical capabilities, and other characteristics that they carry with them separately

and in the sharing, these 'iron oxides' (ferrite) have various and unobjectionable requirements. [1]. The numerous applications that meet global demand in the fields of magnetic fluid technology, nano-electronic chips used in mobile/computers, gas sensor devices, microwave technology, transformer core, transducer, nano SMPS, motor, and dynamo [2–4]. Spinel ferrite is used in significant diagnostic equipment in the medical field. In addition, ferrite has accepted new challenges in the construction of circulators, power equipment, memory devices, and other electronic components. Ferrites perform admirably as a performance enhancer in current energy storage devices such as electrodes of electrochemical cells, exchangers, transporters, and so on. Magnetic spinel ferrite has overcome biocompatibility issues in biotechnology and medical science [5]. They worked efficiently in biosensing devices, isolators, phase shifters, MRI, spintronics, etc. [6, 7]. Ferrites' spontaneous physical and chemical qualities make them suitable for a wide range of applications, including pharmaceuticals, agriculture, industry, and home wastewater treatment. The spinel ferrites' synergistic impact is extended to the design and processing of novel materials. The progress of spinel ferrites in electromagnetic interference shielding is well documented. Spinel ferrite is also well-suited to innovative applications such as magnetic absorbents and photo-catalysts etc. [8, 9]. The spinel ferrites have a cubic lattice structure that can be expressed with a general formula AB_2O_4 [10]. Many academics from all over the world have struggled with the geometric engineering of the spinel's dynamic crystal structure. The crystal lattice's nomenclature belongs to the space group Fd_{3m}-O_h^7; involved tetrahedral (A)-site and octahedral (B)-site, in partnership with the Fe^{3+} ions [11]. The ferrite structure has eight tetrahedral gaps, which are inhabited by trivalent ferrous ions (Fe^{3+} ions), and sixteen octahedral voids occupied in combination by trivalent ferric ions (Fe^{3+} ions) and divalent metal ions viz. Ni^{2+}, Co^{2+}, Cu^{2+}, Mg^{2+}, Mn^{2+}, Ca^{2+}, Zn^{2+} etc. [12]. In this category, nickel ferrite ($NiFe_2O_4$) is a soft ferrite with, inverse spinel [13, 14]. Various synthesis methods have been designed for research and commercial purposes in order to improve the performance chart, achieve new results, and fulfil the application pyramid of these ferrites. Some of the special synthesis methods are sol-gel auto-combustion [15], electro-deposition method [16], co-precipitation method [17], micro-emulsion [18], auto-clave method [19], salt-melt technique [20], spray pyrolysis [21], solid-state reaction method [22], and so on. The term 'additive' refers to a material that is mixed with another substance. An additive is a chemical compound that is added to a target material to increase its physical or chemical qualities while preserving the material's basic properties. Fillers, plasticizers, lubricants, colourants, and other additives must be stable in production conditions, non-toxic, and stable during use while taking availability and cost into consideration. The adding of additives to materials improves bulkiness, mechanical characteristics, chemical properties, optical properties, and rheological properties. To achieve a desired change in physical properties, the addition of such additives is limited to a modest amount in compared to the host substance.

Spinel ferrite's physico-chemical characteristics can be tuned by adding various chemicals to it. Several oxides like niobium oxide (Nb_2O_5), vanadium pentoxide (V_2O_5), tungsten (IV) oxide (WO_2), Lithium carbonate (Li_2CO_3), Bismuth(III) oxide (Bi_2O_3), Cobalt oxide (Co_2O_3) etc. are used as additives [23]. The chemical element vanadium has the symbol V and the atomic number 23. It's a transition metal that's hard, silvery grey, ductile, and malleable. Vanadium is a metal that is rarely discovered in nature and is thought to be poisonous, medium-hard, and ductile. It's a steel-blue transition metal with electrical conductivity and thermal insulator characteristics at its core. Vanadium is rarely discovered in its natural state, but the creation of an oxide layer passivates the free metal against further oxidation once it is isolated chemically. In 1801 in Mexico, Andrés Manuel del Ro incorrectly identified the components of an idea by examining a new mineral called erythronium [24]. Niels Gabriel Sefstrom was persuaded to show the existence of a new element, which he termed vanadium, a few years later in 1830 [25]. Unlike gold, silver, or even nickel, vanadium is widely used in a variety of items and construction materials. Vanadium is an important component in its major application, which is steel strengthening. It can be found in buildings and bridges all around the world, as well as vanadium redox batteries. In Quebec, Canada, roughly 500 kilometres north of Montreal, the mining capital of Chicago, one of the world's largest vanadium layers lies barely beneath the surface. Vanadium pentoxide is an inorganic compound with a high degree of oxidation, making it an oxidizing agent. Vanadium has a bcc structure, which means it has an orthorhombic crystal structure. The alloys of V_2O_5 are utilized as surgical instruments and tools, steel additives, ferrovanadium, vehicle crankshafts, axels, and dental implants due to their non-magnetic nature [26, 27]. Many researchers are reporting the need of V_2O_5 in the materials designing and applications in the various fields. Currently, Xiang Zhang et.al has reported in his literature about the high rate capability along with the ultralong cycle life densification role of free-standing V_2O_5/VG cathodes in their literature [28]. M Samir Ullah et. al has discussed about the concentration effect of V_2O_5 on the structural and magnetic properties of Ni–Co–Zn [29]. Recently, B. Deka Boruah et al. has studied the V_2O_5 cathodes used in the light rechargeable lithium-ion batteries. Kezhuo Li et. al have mentioned in their report the V_2O_5 effect on the porous ceramics [30]. Tarik T. Issa and Samara J. Mohammad has shown V_2O_5 as a candidate for the compacted composites ceramics Yttrium oxide 80 wt.% [31]. The structural, electrical, and magnetic properties of $Ni_{0.7}Zn_{0.3}Fe_2O_4$ + 0.8 wt%V_2O_5 were studied after spinel ferrite was produced using the ceramic method.

2 Experimental

2.1 Synthesis of $Ni_{0}.7Zn_{0}.3Fe_2O_4$ + 0.8 wt%V_2O_5

For the initial starting materials, a high purity $\geq$ 99.9% metal oxides like nickel oxide (NiO); zinc oxide (ZnO); ferric oxide (Fe_2O_3), and vanadium oxide (V_2O_5) were used for the ceramic synthesis. Nickel zinc spinel ferrite of chemical formula $Ni_{0.7}Zn_{0.3}Fe_2O_4$ + 0.8 wt%V_2O_5 was prepared via ceramic method using mortal pestle and milling technique. The essential requirement for making the initial mixture of the selected oxides of all the initial compositions was weighed according to their molar ratios by a weighting machine. The mixture was homogenized using the agate mortar and pestle and ground with the help of a grinder. An obtained $Ni_{0.7}Zn_{0.3}Fe_2O_4$ + 0.8 wt%V_2O_5 as kept for heating at the temperature of 200°C aiming to the remove of moisture. Then thoroughly mixed powder $Ni_{0.7}Zn_{0.3}Fe_2O_4$ + 0.8 wt%V_2O_5 again kept for calcination at 900°C for the period of 24 h. The gained powder was again grounded for 3 h for better crystallization and tuning the crystallite size. This powder was pressed into small pellets shaped in a disc with the dimension of 10×3 mm using a hydraulic press. Polyvinyl alcohol (PVA) was dropped in the prepared mixture to bind the molecular structure of the synthesized material, which can be then used for the pellet formation. The complete sintering process was carried out at a higher temperature at 1080°C held in the alumina crucible in the programmable furnace for 6 h. The final yield product $Ni_{0.7}Zn_{0.3}Fe_2O_4$ + 0.8 wt%V_2O_5 in a powder form was obtained.

2.2 Characterization techniques

The X-ray diffraction pattern of $Ni_{0.7}Zn_{0.3}Fe_2O_4$ + 0.8 wt%V_2O_5 was taken by using Cu-kα radiation ($\lambda = 1.54056$) on (Bruker X-Advanced D8) X-ray diffractometer. The XRD parameters were characterized at room temperature operated at 20 mA current 40 kV voltage. The full X-ray diffraction pattern was produced through ceramic technique was recorded in the 2θ range of 20° to 80° at a scanning rate of 0.01 deg/min, and the primary Bragg's reflections were recorded for structural parameter analysis. The infrared spectroscopy was recorded by NICOLET-NEXU-870 spectrometer using KBr pellet at room temperature in the wavenumber range of 0 cm^{-1} – 4000 cm^{-1}. The IR spectroscopy of the $Ni_{0.7}Zn_{0.3}Fe_2O_4$ + 0.8 wt%V_2O_5 sample was carried out for the determination of functional group analysis. The structural behaviour and phase development were reported from the IR spectra by examining the various stretching vibrations inside the lattice structure. The pulsed-field hysteresis loop tracer (PFHL) supplied by MAGNETA Pvt. Ltd. Mumbai was used to measure the magnetic properties of the samples at room temperature. The applied magnetic field during measurements was +5000 Oe.

3 Results and Discussions

3.1 Structural analysis

The study of crystal structure The X-ray diffraction (XRD) technique was used to examine $Ni_{0.7}Zn_{0.3}Fe_2O_4$ + 0.8 wt%V_2O_5 produced through ceramic process. X-ray diffraction is now utilized to characterise a wide range of materials, including single-crystal epitaxial thin films, polycrystal and powder combinations, and even randomly oriented amorphous materials. X-ray diffraction aids scientists in the development of new pharmaceuticals, the classification of rock formations based on their mineral components, and the understanding of how atom arrangement affects the behaviour of energy storage materials scientists, pushing their ability to engineer materials on an atomic level. In X-ray diffraction, the sample is put in the centre and irradiated by an X-ray beam that moves in a coordinated motion through the detector. The signals from the sample were plotted on a graph, with the peaks corresponding to the material's atomic structure. Typically, crystals are made up of a regular arrangement of atoms, with each atom consisting of a nucleus surrounded by an electron cloud. Because an X-wavelength ray's is similar to the atomic diameter in a lattice. Diffraction happens when x rays interact and is caused by the distance between the atoms in a crystal. It may be used to determine the distance between the atoms in a crystal. When the waves are aligned, the signal is amplified, resulting in constructive interference. When the waves are out of phase, the signal is lost, resulting in destructive interference. Elastic scattering took place, resulting in a repeating pattern of atoms or flakes separated by well-defined distances. The atomic planes scatter X-rays when they are exposed to them. Theta (θ) is the angle formed by the incident and dispersed particles. The scattered waves must be in phase, which means the second wave must travel the same number of wavelengths as the first. One-half of the wavelength is travelled on the incident side, while the other half is travelled on the scattered side in this scenario. There are no impurities in the identified strong peaks in the XRD patterns. All the values of Miller indices (hkl), Bragg's angle (2θ), $\sin\theta$, $\sin\theta/\lambda$ interplanar spacing (d), and intensity of various reflections of $Ni_{0.7}Zn_{0.3}Fe_2O_4$ + 0.8 wt%V_2O_5 are tabulated in Table 1.

The XRD peaks and the peak data have indicated the formation of the complete ferrite phase of the $Ni_{0.7}Zn_{0.3}Fe_2O_4$ + 0.8 wt%V_2O_5 sample. The presence of planes (220), (310), (311), (222), (400), (422), (511), and (440) in the XRD pattern confirmed the creation of single-phase; cubic geometry; spinel structure of the prepared $Ni_{0.7}Zn_{0.3}Fe_2O_4$ + 0.8 wt%V_2O_5 sample, as shown in Figure 1. Assuming that the vanadium oxide form melts around 670°C and forms a liquid phase. When a V_2O_5 additive is added to nickel-zinc ferrite, it improves the mass transport mechanism and generates a liquid phase during sintering. "The incorporation of V^{5+} ions into the spinel crystals of ferrite creates various com-

Table 1. Miller indices (hkl), Bragg's angle (2θ), $\sin\theta$, $\sin\theta/\lambda$, interplanar spacing (d), and intensity of various reflections of $Ni_{0.7}Zn_{0.3}Fe_2O_4$ + 0.8 wt%V_2O_5

(hkl)	2θ (deg)	θ (deg)	$\sin(\theta)$	$\sin\theta/\lambda$	d (Å)	I (a.u)	I/I_0
(220)	30.24	15.12	0.261	0.169	2.952	6025	55.088
(310)	33.24	16.62	0.286	0.186	2.692	4016	36.719
(311)	35.6	17.8	0.306	0.198	2.519	10937	100
(222)	37.26	18.63	0.319	0.207	2.411	3637	33.254
(400)	43.3	21.65	0.369	0.24	2.087	4550	41.602
(422)	53.68	26.84	0.452	0.293	1.706	4258	38.932
(511)	57.18	28.59	0.479	0.311	1.609	5662	51.769
(440)	62.78	31.39	0.520	0.338	1.479	6216	56.835

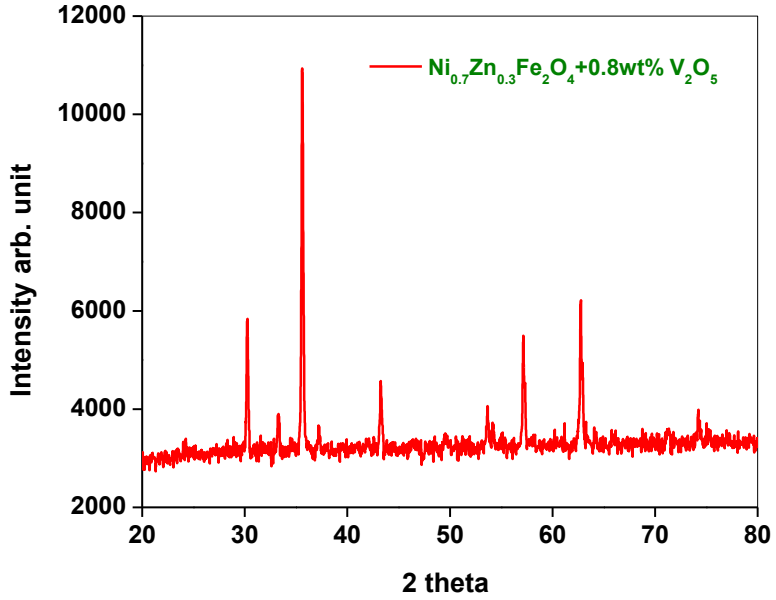

Figure 1. X-ray diffraction of $Ni_{0.7}Zn_{0.3}Fe_2O_4$ + 0.8 wt%V_2O_5.

Table 2. Hopping length L_A, L_B, tetrahedral bond d_{AX} octahedral bond d_{BX} tetra edge d_{AXE}, octa edge d_{BXE} and octa edge unshared d_{BXEu} of $Ni_{0.7}Zn_{0.3}Fe_2O_4$ + 0.8 wt%V_2O_5

L_A (Å)	L_B (Å)	d_{AX} (Å)	d_{BX} (Å)	d_{AXE} (Å)	d_{BXE} (Å)	d_{BXEu} (Å)
3.628	2.962	1.814	2.093	2.962	2.962	2.961

plicated structures in the system, such as the production of Fe^{2+} ions and the precipitation of Fe_2O_3 as the second phase of partial completion of the ferrite phase," according to some literature. The values of Hopping length L_A, L_B, tetrahedral bond d_{AX} octahedral bond d_{BX} tetra edge d_{AXE} octa edge $d_{BXE,}$ and octa edge unshared d_{BXEu} of $Ni_{0.7}Zn_{0.3}Fe_2O_4$ + 0.8 wt%V_2O_5 are given in Table 2.

The avg. lattice constants (a) for the $Ni_{0.7}Zn_{0.3}Fe_2O_4$ +0.8 wt%V_2O_5 spinel ferrite was calculated using the following standard relation:

$$a = d_{hkl}\sqrt{h^2 + k^2 + l^2}\ , \tag{1}$$

where d_{hkl} the interplanar spacing of two planes, (a) is the lattice constant, and (hkl) is the Miller indices of each plane. The avg. lattice parameter (a) for $Ni_{0.7}Zn_{0.3}Fe_2O_4$ + 0.8 wt%V_2O_5 is $a = 8.380$ Å. According to the observations, the value of the lattice parameter over the V_2O_5 doping does not change to as much extend; and could be considered to be unchanged [32]. Also, V^{5+} ions have a smaller radius (0.59 Å) than that of the Fe^{3+} ions (0.64 Å) and Ni^{2+} ions (0.69 Å), the incorporation of V_2O_5 into lattice results in the creation of some Fe^{2+} ions which have an ionic radius (0.74 Å) [33]. The crystallite size of $Ni_{0.7}Zn_{0.3}Fe_2O_4$ + 0.8 wt%V_2O_5 was calculated by using the Debye-Scherrer method taking (311) plane of maximum intensity, which is mentioned by

$$t = \frac{k\lambda}{\beta cos\theta}\ , \tag{2}$$

where λ is the X-ray wavelength, β is the full width at half maximum, θ is Bragg's angle, and $k = 0.89$. An average crystallite size (t) obtained from XRD data for 0.8 wt%V_2O_5 doped $Ni_{0.7}Zn_{0.3}Fe_2O_4$ was found to be higher in comparison. The X-ray density (d_X) of $Ni_{0.7}Zn_{0.3}Fe_2O_4$ + 0.8 wt%V_2O_5 was calculated by the following relation:

$$d_X = 8M/(N_A^3)\ , \tag{3}$$

where M is the molecular weight and N_A is the Avogadro's number, α is lattice constant. The X-ray density for $Ni_{0.7}Zn_{0.3}Fe_2O_4$ + 0.8 wt%V_2O_5 was obtained as 5.303 g/cm^3. The porosity was found to be 22.60% which was according to the expectations. The values of the structural parameters like lattice parameter α, X-ray density d_X, bulk density d_B, volume V, and porosity P% of $Ni_{0.7}Zn_{0.3}Fe_2O_4$ + 0.8 wt%V_2O_5 are depicted in Table 3.

Table 3. Lattice parameter α (Å), X-ray density d_X(g/cm^3), bulk density d_B (g/cm^3), volume V, and porosity P (%), and crystallite size of $Ni_{0.7}Zn_{0.3}Fe_2O_4$ + 0.8 wt%V_2O_5

α (Å)	d_X (g/cm^3)	d_B (g/cm^3)	V (Å^3)	P (%)	t
8.380	5.336	4.109	588.55	22.60	2.694

3.2 Infrared spectroscopy

The IR spectroscopy confirmed the functional group present and the bands associated with the $Ni_{0.7}Zn_{0.3}Fe_2O_4$ + 0.8 wt%V_2O_5. According to Waldron's research, the IR spectra of ferrite must be interpreted as continuously attached crystals [34]. As seen in Figure 2, the IR absorption bands of $Ni_{0.7}Zn_{0.3}Fe_2O_4$ + 0.8 wt%V_2O_5 are assigned to the vibration of metal ions (M-O) in the crystal lattice. The high-frequency band υ_1 (542 cm^{-1}) correspond to the intrinsic vibration of the tetrahedral group complexes Fe^{3+}–O^{2-} and υ_2 (410.84 cm^{-1}) corresponds to the octahedral group complexes Fe^{3+}–O^{2-}.

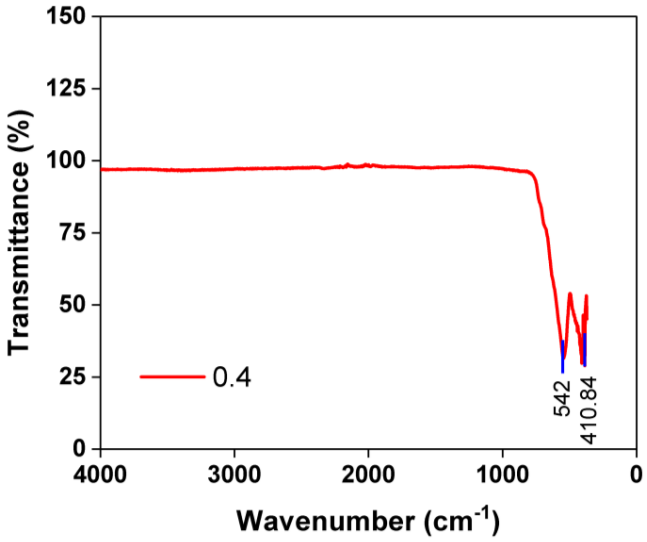

Figure 2. Infra-red spectra of $Ni_{0.7}Zn_{0.3}Fe_2O_4$ + 0.8 wt%V_2O_5.

3.3 DC-electrical resistivity

DC-electrical resistance was recorded by two probe methods in the temperature range 1000–2000 K^{-1}.

The DC-resistivity of $Ni_{0.7}Zn_{0.3}Fe_2O_4$ + 0.8 wt%V_2O_5 was calculated by standard formula

$$\rho = RA/t\,, \tag{4}$$

where R is the resistance, t is the thickness of the sample, and $A = \pi r^2$ is the area of the electrode in contact. The logarithm of DC-resistivity versus $1000/T$ (K^{-1}) temperature of $Ni_{0.7}Zn_{0.3}Fe_2O_4$ + 0.8 wt%V_2O_5 is shown in Figure 3 revealing the resistive property and marked a fall in resistivity with

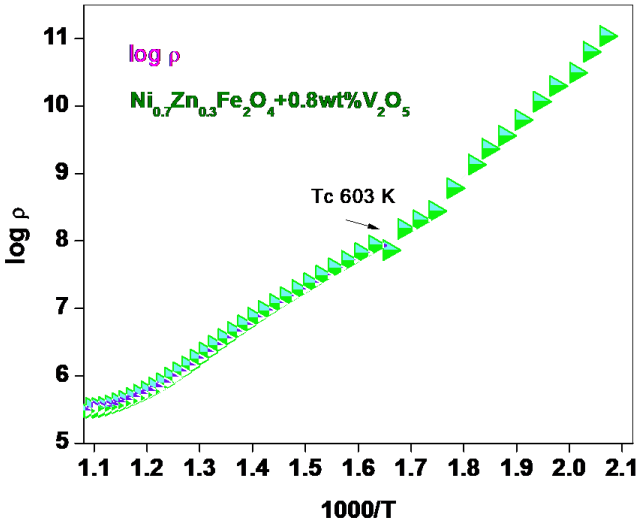

Figure 3. Temperature dependence DC-resistivity of $Ni_{0.7}Zn_{0.3}Fe_2O_4$ + 0.8 wt%V_2O_5.

hiking the temperature obeying the Arrhenius law [35]. Following the semiconducting characteristic of the material, increasing temperature causes the graph of DC-resistivity to decrease.

3.4 Magnetic property

The important magnetic parameters of $Ni_{0.7}Zn_{0.3}Fe_2O_4$ + 0.8 wt%V_2O_5 synthesized via ceramic method were determined using the pulse field hysteresis loop tracer technique on the device MAGNETA, at room temperature (see Figure 4). The applied magnetic field was kept at 5000 Oe. The values of saturation magnetization (M_s), remanence magnetization (M_r), and coercivity (H_c) were determined for $Ni_{0.7}Zn_{0.3}Fe_2O_4$ + 0.8 wt%V_2O_5 and $Ni_{0.7}Zn_{0.3}Fe_2O_4$ [23] are depicted in Table 4. It was found that the saturation magnetization (M_s) and remanence magnetization (M_r“) over the addition of 0.8 wt%V_2O_5 were recorded

Table 4. Saturation magnetization (M_s), remanence magnetization (M_r), and coercivity (H_c), magnetic remanence to saturation ratio (M_r/M_s), and magneton number for $Ni_{0.7}Zn_{0.3}Fe_2O_4$ + 0.8 wt%V_2O_5

	M_s (emu/gm)	M_r (emu/gm)	H_c (Oe)	M_r/M_s	n_B (μb)
$Ni_{0.7}Zn_{0.3}Fe_2O_4$ + 0.8 wt%V_2O_5	79.11	2.44	75.24	33.84	2.576
$Ni_{0.7}Zn_{0.3}Fe_2O_4$ [23]	74.60	2.26	18.71	33.00	2.429

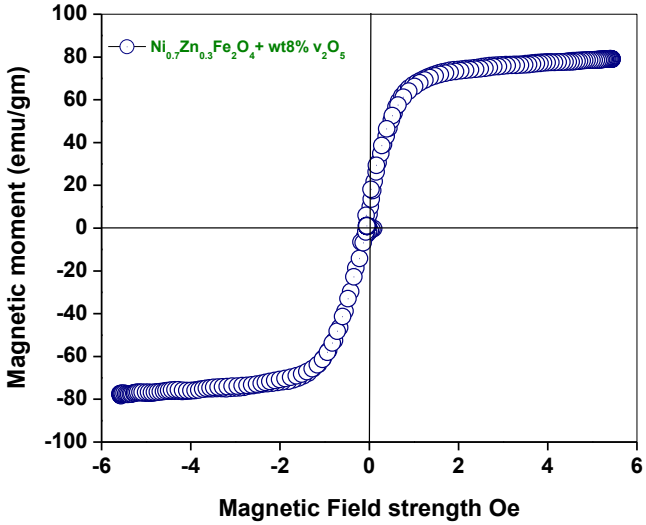

Figure 4. M–H curve of magnetization for $Ni_{0.7}Zn_{0.3}Fe_2O_4$ + 0.8 wt%V_2O_5.

to be increased in comparison to the $Ni_{0.7}Zn_{0.3}Fe_2O_4$ [23]. A drastic change in the coercivity (H_c) value was seen as an effect of 0.8 wt%V_2O_5.

4 Conclusions

The ceramic approach was used to make $Ni_{0.7}Zn_{0.3}Fe_2O_4$ + 0.8 wt%V_2O_5 in this study. The standard formula was used to determine the structural values acquired from X-ray diffraction data. The inverse type, single-phase, cubic spinel ferrite structure of $Ni_{0.7}Zn_{0.3}Fe_2O_4$ + 0.8 wt%V_2O_5 produced using ceramic technique has been validated. The lattice constant was reported as 8.380 Å, which is consistent with the literature and was found to be unaffected by the addition of 0.8 wt%V_2O_5. The X-ray density (d_X) of $Ni_{0.7}Zn_{0.3}Fe_2O_4$ + 0.8 wt%V_2O_5 was obtained to be 5.336 g/cm^3. Hopping length L_A, L_B, tetrahedral bond d_{AX}, octahedral bond d_{BX}, tetra edge d_{AXE}, octa edge d_{BXE}, and octa edge unshared d_{BXEu} of $Ni_{0.7}Zn_{0.3}Fe_2O_4$ + 0.8 wt%V_2O_5 were derived from the XRD data which are following the reported range in literature. The infrared spectroscopy (IR) has confirmed the ferrite phase formation in $Ni_{0.7}Zn_{0.3}Fe_2O_4$ + 0.8 wt%V_2O_5. The logarithmic plot of DC-resistivity has suggested the semiconducting behavior of $Ni_{0.7}Zn_{0.3}Fe_2O_4$ + 0.8 wt%V_2O_5. Also, an increase in saturation magnetization (M_s), remanence magnetization (M_r), and magneton number (n_B) of $Ni_{0.7}Zn_{0.3}Fe_2O_4$ + 0.8 wt%V_2O_5 have been recorded which may suit several application areas.

References

[1] M.A. Rafiq, A. Javed, M.N. Rasul, M.A. Khan, A. Hussain (2020) Understanding the structural, electronic, magnetic and optical properties of spinel MFe2O4 (M = Mn, Co, Ni) ferrite.*Ceram. Int.* **46** 4976-4983.

[2] K. Srinivasamurthy, S. Kubrin, S. Matteppanavar, D. Sarychev, P.M. Kumar, H.W. Azale, B. Rudraswamy (2015) Tuning of ferrimagnetic nature and hyperfine interaction of Ni2+ doped cobalt ferrite nanoparticles for power transformer applications. *Ceram. Int.* **44** 9194-9203.

[3] M. Abdollahi, S. Manouchehri, M. Yousefi (2022) A new nano-grain Mn-Zn spinel ferrite smart cores to enhance the efficiency of high-frequency devices. *Indian J. Phys.* **96** 1405–1411.

[4] S. Shaat, H. Dawoud (2021) Influence of variation of structural parameters on magnetic properties of Al-substituted Ni spinel ferrite. *J. Mater. Sci. Mater. Electron.* **32** 11536-11546.

[5] M. Rethinasabapathy, A.E. Vilian, S.K. Hwang, S.-M. Kang, Y. Cho, Y.-K. Han, J.-K. Rhee, Y.S. Huh (2021) Cobalt ferrite microspheres as a biocompatible anode for higher power generation in microbial fuel cells. *J. Power Sources* **483** 229170.

[6] C. Murugesan, K. Ugendar, L. Okrasa, J. Shen, G. Chandrasekaran (2021) Zinc substitution effect on the structural, spectroscopic and electrical properties of nanocrystalline MnFe2O4 spinel ferrite. *Ceram. Int.* **47** 1672-1685.

[7] H. Kosaki, M. Umeda, E. Saitoh, Y. Shiomi (2021) Magnon–Photon Coupling in a Spinel Ferrite with Large Gilbert Damping. *J. Phys. Soc. Japan* **90** 083702.

[8] I.A. Amar, S. Faraj, M. Abdulqadir, I. Abdalsamed, F. Altohami, M. Samba (2021) Oil Spill Removal from Water Surfaces using Zinc Ferrite Magnetic Nanoparticles as A Sorbent Material. *Iraqi J. Sci.* **62** 718-728.

[9] G. Padmapriya, S.S. Iqbal (2020) Facile Synthesis and Opto-Magnetic Characterization Studies of Nano structured Photo catalysts for the Degradation of Azo Dyes. *Malaya Journal of Matematik* **S**(2) 2344-2346

[10] N. Younis, M. Abd-Elrahman, N. Afify, A.A. El-Fadl, A. Abu-Sehly (2021) Structural, optical and magnetic characterizations of nanoparticles spinel Zn(1-x)MxAl2O4 (M = Co and Ni) synthesized by microwave combustion method. *J. Mater. Sci. Eng., B* **271** 115316.

[11] M. Gupta, A. Sinha, S. Kanetkar, S. Date, A. Nigavekar (1979) Evidence of electron exchange between Fe2+ and Fe3+ ions on tetrahedral and octahedral sites in Fe2MoO4. *J. Phys. C* **12** 2401.

[12] P. Anantharamaiah, B.P. Rao, H. Shashanka, J. Chelvane, V. Khopkar, B. Sahoo (2021) Role of Mg2+ and In3+ substitution on magnetic, magnetostrictive and dielectric properties of NiFe2O4 ceramics derived from nanopowders. *Phys. Chem. Chem. Phys.* **23** 1694-1705.

[13] G. Pratibha, A. Thirupathi, V.V. Krishna, P.S. Kumar, G.S.S. Yadav (2021) Effect of Ni substitution on structural, dielectric and magnetic properties of Zn ferrite nanoparticles. *J. Ovonic Res.* **17** 323-331.

[14] P. Ramakrishnan, K.B. Lee, G.-J. Choi, I.-K. Park, J.I. Sohn (2021) Porous hollow nanorod structured chromium-substituted inverse spinel compound: An efficient oxygen evolution reaction catalyst. *J. Ind. Eng. Chem.* **101** 178-185.

[15] R. Zakir, S.S. Iqbal, A.U. Rehman, S. Nosheen, T.S. Ahmad, N. Ehsan, F. Inam (2021) Spectral, electrical, and dielectric characterization of Ce-doped Co-Mg-Cd spinel nano-ferrites synthesized by the sol-gel auto combustion method. *Ceram. Int.* **47** 28575-28583.

[16] T. Baskar, A.S. George, B. Aremu (2020) Effect of different concentration of boron on properties of electroplated nickel-boron alloy thin films. *J. Inf. Comput. Sci.* **10**(05) 853-861.

[17] A.A. Ati, A.H. Abdalsalam, A.S. Hasan (2021) Thermal, microstructural and magnetic properties of manganese substitution cobalt ferrite prepared via co-precipitation method, *J. Mater. Sci. Mater. Electron.* **32** 3019-3037.

[18] M.A. Khan, M.Q. uz Zaman, A. Majeed, M.N. Akhtar, W. Abbas (2021) Structural, spectral, dielectric and magnetic properties of Sr2CuxNi2-xFe28-xCrxO46 ($0 \leq x \leq 0.5$) ferrites synthesized via micro-emulsion route. *Mater. Chem. Phys.* **259** 124066.

[19] M.B. Tahir (2021) Construction of visible light driven CuBi2O4/Bi2WO6 solid solutions anchored with Bi12O17ClxBr2–x nanoparticles for improved photocatalytic activity. *Ceram. Int.* **47** 320-328.

[20] M. Chen, Y.X. Yin, M.L. Qi, Y.L. Ding, Y.M. Wang (2021) Effect of Reaction Time on the Coercivity of Barium Ferrite Synthesized by Hydrothermal Process. In: Materials Science Forum, Trans. Tech. Publ., pp. 687-691.

[21] S.B. Narang, K. Pubby, Nickel spinel ferrites: A review (2021) *J. Magn. Magn. Mater.* **519** 167163.

[22] L. Zhang, Y. Wang, B. Liu, J. Wang, G. Han, Y. Zhang (2021) Characterization and property of magnetic ferrite ceramics with interesting multilayer structure prepared by solid-state reaction. *Ceram. Int.* **47** 10927-10939.

[23] A. Alshoaibi (2020) Effective optical nanoparticles and nanocomposites based on a carbon nanotubes-organic-inorganic nanohybrid for industrial pollutant removal. *Mater. Express* **10** 856-865.

[24] D. Rabinovich (2021) The Periodic Table at 150: A Philatelic Celebration. In: 150 Years of the Periodic Table, Springer, pp. 439-449.

[25] D. Rehder (2008) "Bioinorganic vanadium chemistry". John Wiley & Sons.

[26] S. Uysal (2020) Coal ashes as a vanadium resource and its potential in Turkey. Bachalor Thesis. Dokuz Eylul University.

[27] A.J. Allen, I. Levin, S.E. Witt (2020) Materials research & measurement needs for ceramics additive manufacturing. *J. Am. Ceram. Soc*. **103** 6055-6069.

[28] X. Zhang, Y. Tang, P. He, Z. Zhang, T. Chen (2021) Edge-rich vertical graphene nanosheets templating V2O5 for highly durable zinc ion battery. *Carbon* **172** 207-213.

[29] M.S. Ullah, M.F. Uddin, A. Momin, M. Hakim (2021) Effect of V2O5 addition on the structural and magnetic properties of Ni–Co–Zn ferrites. *Mater. Res. Express* **8** 016102.

[30] K. Li, S. Ge, G. Yuan, H. Zhang, J. Zhang, J. He, Q. Jia, S. Zhang (2021) Effects of V2O5 addition on the synthesis of columnar self-reinforced mullite porous ceramics. *Ceram. Int.* **47** 11240-11248.

[31] T.T. Issa, S.J. Mohammad (2021) Sintering Additives Effects on the Microstructure and Electrical Behavior of Yttrium Oxide Ceramic Composites, *NeuroQuantology* **19** 62.

[32] M. Patil, M. Sarnaik, V. Murumkar, A. Pandit, D. Shingule (2017) Effect of V2O5 Additive on Structural and Magnetic Properties of Ni-Zn ferrite. *Int. Adv. Res. J. Sci. Eng. Technol.* **4** 58-62.

[33] M. Kaiser (2010) Influence of V2O5 ion addition on the conductivity and grain growth of Ni–Zn–Cu ferrites. *Curr. Appl. Phys.* **10** 975-984.

[34] R. Waldron (1955) Infrared spectra of ferrites. *Phys. Rev.* **99** 1727.

[35] S. Mahboob, G. Prasad, G. Kumar (2021) Dielectric, impedance and resistivity studies on [Ba (Nd0. 1Ti0. 8Nb0. 1) O3] 0.40 [(Na0. 5Bi0. 5) TiO3] 0.40 [CaTiO3] 0.20 piezoelectric ceramic. *J. Mater. Sci. Eng., B* **263** 114823.